JACS Au
AN OPEN ACCESS JOURNAL OF THE AMERICAN CHEMICAL SOCIETY

pubs.acs.org/jacsau
Article

Mechanistic Insights into Nitrile Activation by Cobalt(III)−Hydroperoxo Intermediates: The Influence of Ligand Basicity

Yeongjin Son, Donghyun Jeong, Kyungmin Kim, and Jaeheung Cho*

Cite This: *JACS Au* 2023, 3, 3204−3212
Read Online

ACCESS | Metrics & More | Article Recommendations | Supporting Information

ABSTRACT: The versatile applications of nitrile have led to the widespread use of nitrile activation in the synthesis of pharmacologically and industrially valuable compounds. We reported the activation of nitriles using mononuclear cobalt(III)−hydroperoxo complexes, $[Co^{III}(Me_3\text{-TPADP})(O_2H)(RCN)]^{2+}$ [R = Me (**2**) and Ph ($\mathbf{2}^{Ph}$)], to form cobalt(III)−peroxyimidato complexes, $[Co^{III}(Me_3\text{-TPADP})(R{-}C(=NH)O_2)]^{2+}$ [R = Me (**3**) and Ph ($\mathbf{3}^{Ph}$)]. The independence of the rate on the nitrile concentration and the positive Hammett value of 3.2(2) indicated that the reactions occur via an intramolecular nucleophilic attack of the hydroperoxide ligand to the coordinated nitrile carbon atom. In contrast, the previously reported cobalt(III)−hydroperoxo complex, $[Co^{III}(TBDAP)(O_2H)(CH_3CN)]^{2+}$ ($\mathbf{2}^{TBDAP}$), exhibited the deficiency of reactivity toward nitrile. The comparison of pK_a values and redox potentials of **2** and $\mathbf{2}^{TBDAP}$ showed that Me_3-TPADP had a stronger ligand field strength than that of TBDAP. The density functional theory calculations for **2** and $\mathbf{2}^{TBDAP}$ support that the strengthened ligand field in **2** is mainly due to the replacement of two *tert*-butyl amine donors in TBDAP with methyl groups in Me_3-TPADP, resulting in the compression of the Co−N_{ax} bond lengths. These results provide mechanistic evidence of nitrile activation by the cobalt(III)−hydroperoxo complex and indicate that the basicity dependent on the ligand framework contributes to the ability of nitrile activation.

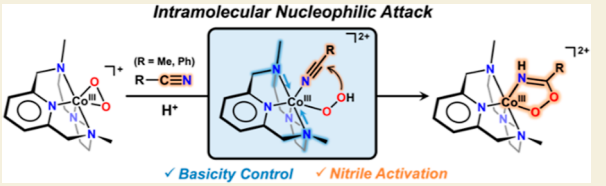

KEYWORDS: *bioinorganic chemistry, nitrile activation, cobalt−hydropeoxo, basicity control, reactivity modulation*

INTRODUCTION

The functionalization of nitriles has attracted considerable interests in the fields of synthetic and pharmaceutical chemistry because nitrile compounds are highly multipurposed precursors for diverse functional groups.[1,2] However, due to the stability of nitrile possessing a strong C≡N bond, the classical methods to activate nitriles have exhibited several disadvantages such as high energy demands and harsh conditions.[3−6] Thus, the accomplishment of the nitrile activation under mild conditions has been considered a challenging task.[7,8] Inspired by the cobalt- or iron-containing nitrile hydratase, the studies on the functionalization of nitriles under ambient conditions by transition metal catalysts have shown impressive progresses.[9−18]

Metal−dioxygen species such as metal−(hydro)peroxo [M−O_2(H)] complexes have been invoked as important reactive intermediates for various oxidative reactions in biological systems.[19−24] For examples, numerous M−O_2(H) complexes have been reported to conduct nucleophilic reactions, including aldehyde deformylation in biomimetic models.[25−40] Several M−O_2(H) species have been documented to readily oxidize nitriles under mild conditions (Scheme 1).[41−49] In a rhodium complex with *tert*-butyl isocyanide and triethylphosphine ligands, it was revealed that the rhodium(III)−hydroperoxo intermediate is responsible for the nitrile activation to afford a rhodium(III)−peroxyimidato species (step a).[48] Similarly, the synthesis of a nickel(II)−peroxyimidato complex was achieved by the reaction of a nickel(II) complex bearing a tetradentate cyclam ligand with hydrogen peroxide in CH_3CN.[49] However, the mechanism for the cyclization reaction forming a metal−peroxyimidato complex remains elusive.

Scheme 1. Nitrile Activation by Metal−Dioxygen Complexes

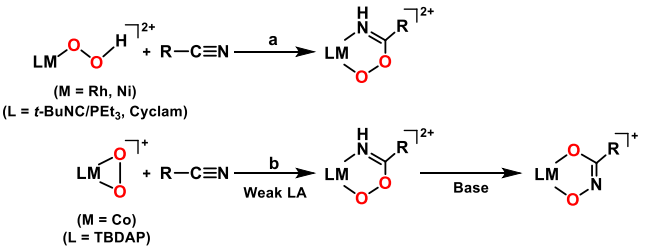

Received: September 8, 2023
Revised: October 6, 2023
Accepted: October 9, 2023
Published: October 31, 2023

The cobalt(III)−peroxo complex with a TBDAP (*N*,*N*′-di-*tert*-butyl-2,11-diaza[3.3](2,6)-pyridinophane) ligand has been implicated as the oxidant for nitrile activation; in the presence of weak Lewis acids, the reactions of the cobalt(III)−peroxo complex and nitriles give cobalt(III)−peroxyimidato complexes (step b).[41−44] Then, the addition of an external base induces the conversion of the cobalt(III)−peroxyimidato complexes to the cobalt(III)−hydroximato complexes.[44] Theoretical studies have suggested that the cobalt(III)−peroxyimidato complex is formed via a nucleophilic attack by the peroxo moiety.[42−44] However, the cobalt(III)−hydroperoxo complex from the conversion of the cobalt(III)−peroxo species by much stronger Lewis acidic metal ions in place of weak Lewis acid additives shows a lack of reactivity toward nitrile.[44] The result is significantly different from the previously reported nitrile activation by M−O_2H complexes and requires further studies for the reaction mechanism.

The difference in reactivity toward nitrile by the M−O_2H complexes (M = Rh, Ni, and Co) may be attributed to the differences in nucleophilicity. The rhodium and nickel complexes feature strong electron-donating ligands such as *tert*-butyl isocyanide/triethylphosphine and cyclam, respectively, leading to higher basicity than that of the cobalt complex with the pyridine-based TBDAP ligand.[44,48,49] The assumption can be rationalized by previous studies stating that the ligand modification of metal−oxygen complexes affected the structural and the chemical properties.[50−55] For example, the *α*-substitution of the pyridine ring in the 6-Me_3-TPA ligand tuned the bond lengths of an iron(II) complex; bulkier methyl substituted pyridine groups gave the elongation of the Fe−N bonds, which showed the weaker basicity than that of the TPA ligand without methyl groups.[50] The iron(III)−peroxo species with an electron-rich porphyrin has been found to be more reactive in terms of nucleophilic reactivity toward electron-poor olefins.[54] Furthermore, the introduction of an axial ligand to a porphyrin iron(III)−peroxo complex has led to a significant increase in the nucleophilic olefin oxidation.[55]

In this context, we examine the reactivity and basicity of cobalt(III)−hydroperoxo complexes supported by TBDAP and Me_3-TPADP (3,6,9-trimethyl-3,6,9-triaza-1(2,6)-pyridinacyclodecaphane) ligands and report herein the nitrile activation by mononuclear cobalt(III)−hydroperoxo complexes, $[Co^{III}(Me_3\text{-TPADP})(O_2H)(RCN)]^{2+}$ [R = Me (**2**) and Ph (**2**^{Ph})]. We reveal that the nitrile activation proceeds through an intramolecular nucleophilic attack of the hydroperoxide ligand to nitrile carbon, producing the cobalt(III)−peroxyimidato complexes $[Co^{III}(Me_3\text{-TPADP})(R{-}C(=NH)O_2)]^{2+}$ [R = Me (**3**) and Ph (**3**^{Ph})] (Scheme 2). The fact that the reactivity of the cobalt(III)−hydroperoxo complex is markedly enhanced upon replacing the TBDAP ligand with Me_3-TPADP suggests that the basicity of Me_3-TPADP is higher than that of TBDAP. The tendency was supported by the thermodynamic factors such as pK_a values and redox potentials of cobalt(III)−hydroperoxo complexes and density functional theory (DFT) studies. These results provide valuable mechanistic insights into nitrile activation by M−O_2(H) intermediates, illuminating the reaction mechanism and the factors governing the reactivity.

Scheme 2. Nitrile Activation of a Cobalt(III)−Hydroperoxo Complex (2) from the Reaction of Cobalt(III)−Peroxo Complex (1) and Nitriles in the Presence of Proton

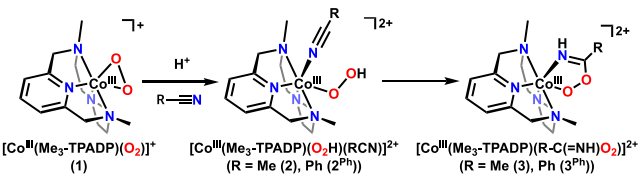

RESULTS AND DISCUSSION

Nitrile Activation of $[Co^{III}(Me_3\text{-TPADP})(O_2H)(CH_3CN)]^{2+}$ (2)

2 was prepared by modifying a previously described method.[56,57] The generation of **2** was carried out from the reaction of the isolated cobalt(III)−peroxo complex, $[Co^{III}(Me_3\text{-TPADP})(O_2)]^+$ (**1**), with 1 equiv of HOTf in CH_3CN/CH_3OH (*v*/*v* = 1:1) at 0 °C, which afforded the characteristic absorption band of **2** at 320 nm (ε = 4100 M^{-1} cm^{-1}) (Figure 1a). The solution changed from purple to magenta. Spectroscopic titration established the stoichiometric conversion of **1** to **2** by HOTf (Figure S1). Then, **2** readily reacted with CH_3CN to give **3** with the disappearance of the characteristic band of **2** and the appearance of a weak absorption band at 630 nm (ε = 320 M^{-1} cm^{-1}) in 88% yield, which exhibited isosbestic points at 414, 455, and 571 nm (Figures 1a and S2). The reaction accompanied the color change from magenta to cyan. In the absence of HOTf, the spectrum of **1** remained unchanged at 0 °C, which indicated that **1** was an ineffective oxidant in nitrile activation (Figure S3). The electrospray ionization mass spectrometry (ESI−MS) spectrum of **3** exhibited a prominent ion peak at a mass-to-charge (*m*/*z*) ratio of 190.5, whose mass and isotope pattern correspond to $[Co(Me_3\text{-TPADP})(CH_3C(=NH)O_2)]^{2+}$ (**3**-^{16}O; calcd. *m*/*z* 190.6) (Figure 1b). When the reaction was executed with $[Co(Me_3\text{-TPADP})(^{18}O_2)]^+$, a mass peak corresponding to $[Co(Me_3\text{-TPADP})(CH_3C(=NH)^{18}O_2)]^{2+}$ (**3**-^{18}O) appeared at *m*/*z* 192.5 (calcd. *m*/*z* 192.6) (Figure 1b, inset). The increase of 4 mass units demonstrated that the oxygen atoms of **3** were derived from the peroxo ligand of **1**. The Fourier-transform infrared (FT-IR) spectrum of **3** showed apparent peaks corresponding to the N−H and C=N vibrations at 3288 and 1636 cm^{-1}, respectively, whose values were comparable to those of the previously reported cobalt(III)−peroxyimidato species (Figure S4).[44]

The characteristic peaks of **3** were further assigned by ^{1}H NMR, carbon nuclear magnetic resonance (^{13}C NMR), ^{1}H−^{1}H homonuclear correlation spectroscopy (COSY), and ^{1}H−^{13}C heteronuclear single quantum coherence (HSQC) in CD_3CN/CD_3OD (*v*/*v* = 1:1) at 0 °C (Figures 1c and S5−S8). The ^{1}H NMR spectrum of **3** showed the characteristic signal associated with the methyl group of the peroxyacetimidate ligand moiety in **3** at 2.43 ppm (Figures 1c and S5). Based on the ^{1}H−^{13}C HSQC experiment, a single cross peak exhibited that a ^{1}H signal at 2.43 ppm correlated with the ^{13}C chemical shift at 16.31 ppm, indicating the presence of a methyl group in the peroxyacetimidate ligand moiety of **3** (Figure 1c, inset and Figure S8). However, the observation of the NH group of imine moiety might be hampered by the fast proton exchange with the solvent.[58−61] The X-band electron paramagnetic resonance (EPR) silence (Figure S9) and the NMR spectral features obviously demonstrated that **3** was a low-spin *S* = 0 cobalt(III)−peroxyimidato complex. The X-ray crystal structure of **3**-$(ClO_4)_2(CH_3CN)_2$ revealed the cobalt(III) center in a distorted octahedral geometry (Figure 2, Tables S1 and S10). The five-membered chelate ring of a peroxyacetimidate ligand

https://doi.org/10.1021/jacsau.3c00532
JACS Au 2023, 3, 3204−3212

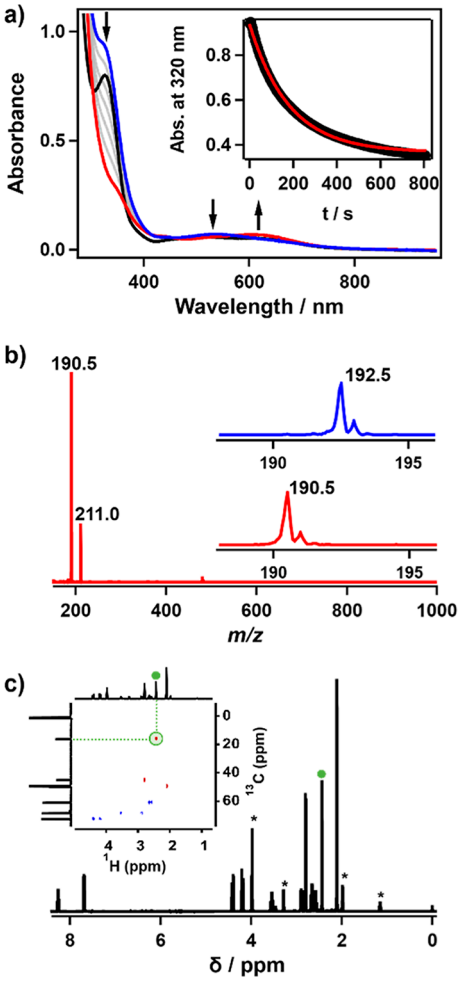

Figure 1. (a) UV−vis spectral changes for the reaction of **1** (0.25 mM, black) in the presence of HOTf (0.25 mM) in CH_3CN/CH_3OH (v/v = 1:1) at 0 °C, which affords **2** (blue) following decay to form **3** (red). Inset shows the time course of the absorption band at 320 nm and its first-order fitting (red line). (b) Electrospray ionization mass spectrometry (ESI−MS) spectrum of **3**. The peak at m/z 190.5 corresponds to **3**-^{16}O. Insets show observed isotope distribution patterns for **3**-^{16}O (red) and **3**-^{18}O (blue). (c) Proton nuclear magnetic resonance (^{1}H NMR) spectrum of **3** (16 mM) in CD_3CN/CD_3OD (v/v = 1:1) at 0 °C exhibits the methyl group of the peroxyacetimidate ligand bound to the cobalt(III) center at 2.43 ppm as a green circle. The peaks marked with "*" are ascribed to solvents. Inset shows the ^{1}H−^{13}C heteronuclear single quantum coherence (HSQC) spectrum including a green cross peak (δ_C = 16.31, δ_H = 2.43) correlating with the methyl group of **3**.

included the N5−Co−O1 angle of 83.64(17)°, arising from the oxidation of carbon in nitrile by the hydroperoxo group. The O1−O2 bond length was 1.482(4) Å, which was similar to those of previously reported peroxyacetimidate cobalt(III) (1.482(3) Å) and rhodium(III) complexes (1.491(2) Å).[44,48] The C1−N5 and C1−O2 bond lengths were 1.284(5) and 1.310(5) Å, respectively, which were comparable to those of other metal−peroxyimidato complexes.[44,48] Furthermore, the hydrogen atom (H1) of the imine moiety was successfully refined (Figure S10). Taken together, these spectroscopic and structural evidence clearly indicated that **3** was a cobalt(III)−peroxyimidato complex, $[Co^{III}(Me_3\text{-TPADP})(CH_3C(=NH)\text{-}O_2)]^{2+}$.

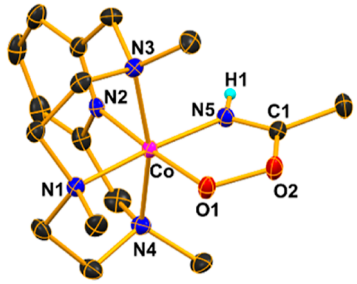

Figure 2. ORTEP of $[Co^{III}(Me_3\text{-TPADP})(CH_3C(=NH)O_2)]^{2+}$ (**3**) with thermal ellipsoids drawn at the 30% probability level. Hydrogen atoms are omitted for clarity, except for a hydrogen atom on the imine moiety.

The absorption spectral titration experiments indicated that an excess of CH_3CN was required for the full formation of **2** (Figure S11). In the presence of 2.4 M CH_3CN in CH_3OH at 0 °C, **2** vanished with a first-order decay profile. Interestingly, the observed pseudo-first-order rate constant (k_{obs} = 5.9(0) × 10^{-3} s^{-1}) was independent of the concentration of CH_3CN (Figure 3a). Activation parameters of the nitrile activation

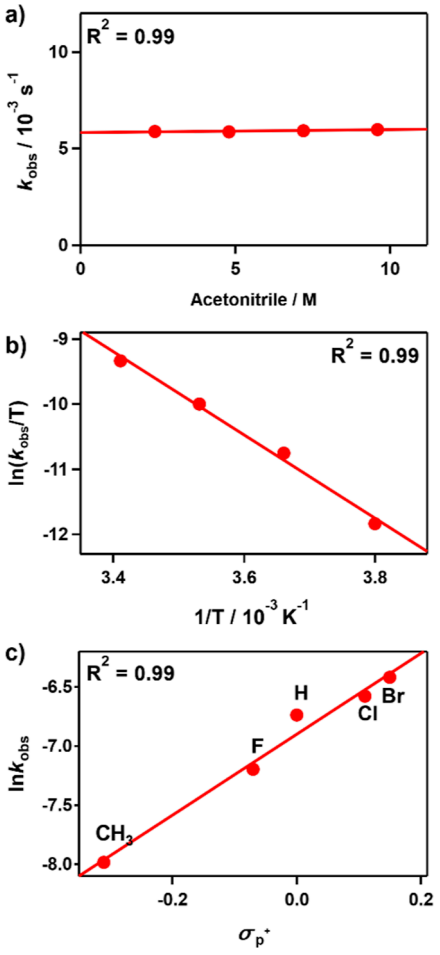

Figure 3. (a) Plot of k_{obs} against CH_3CN concentration obtained in the reaction of **2** (0.25 mM) with CH_3CN to determine a first-order rate constant (k_{obs}) at 0 °C. (b) Plot of first-order rate constants against $1/T$ obtained in the reaction of **2** (0.25 mM) with CH_3CN to determine the activation parameters. (c) Hammett plot of ln k_{obs} against σ_p^+ of benzonitrile derivatives in the reaction of **2** (0.25 mM) with *para*-X−Ph−CN (X = CH_3, F, H, Cl, Br) at 0 °C.

https://doi.org/10.1021/jacsau.3c00532
JACS Au 2023, 3, 3204−3212

from **2** to **3** were determined to be $\Delta H^{\ddagger}$ = 13(1) kcal mol^{-1} and $\Delta S^{\ddagger}$ = −22(2) cal mol^{-1} K^{-1} from an Eyring analysis of temperature-dependent k_{obs} in the range of 263−293 K (Figure 3b). The observed negative entropy value was arising from the highly ordered transition state of the cyclization reaction.[62−65] These kinetic data suggested that the formation of **3** occurred via a unimolecular mechanism (vide infra). The kinetic isotope effect (KIE) value was determined to be 1.0 using CD_3CN, which displayed that the rate-determining step of nitrile activation by **2** was scarcely affected by the C−H bond dissociation energies of the CH_3CN.

When the CH_3CN was replaced with benzonitrile (PhCN) in the optical titration, a cobalt(III)−hydroperoxo species, $[Co^{III}(Me_3\text{-TPADP})(O_2H)(PhCN)]^{2+}$ (**2**^{Ph}), was fully generated at a low concentration of PhCN (Figure S12). Adding HOTf to a solution of **1** in the presence of 0.3 M benzonitrile (PhCN) in $CH_3OH/CHCl_3$ (v/v = 19:1) at 0 °C caused immediate generation of **2**^{Ph}, which converted to the cobalt(III)−peroxybenzimidato complex, $[Co^{III}(Me_3\text{-TPADP})(PhC(=NH)O_2)]^{2+}$ (**3**^{Ph}), in 93% yield with isosbestic points at 401, 455, and 570 nm (Figure S13 for UV−vis and ESI−MS spectra). Further kinetic studies for the formation of **3**^{Ph} in the range of 0.075−0.3 M showed consistent reaction rates regardless of the concentration of PhCN, giving a k_{obs} value of 1.4(1) × 10^{-3} s^{-1} at 0 °C (Figure S14). The reactions of **2** with *para*-substituted benzonitrile derivatives, *p*-X−Ph−CN (X = CH_3, F, H, Cl, and Br), were performed to assess the electronic nature of the $Co^{III}-O_2H$ moiety of **2** in the cyclization reaction. The Hammett plot of the pseudo-first-order rate constants versus σ_p^+ gave a ρ value of 3.2(2) (Figure 3c). The positive ρ value indicated that the cyclization for the cobalt(III)−peroxyimidato complex involved a nucleophilic attack of the hydroperoxide ligand of **2** to the carbon atom of the nitrile group attached to the cobalt center. Kinetic studies provided the first experimental evidence in support of the previously proposed mechanism for nitrile activation by $M-O_2H$.[44,48]

Nitrile Activation of $[Co^{III}(Me_3\text{-TPADP})(O_2)]^+$ (1) by Weak Lewis Acidic Metal Ions

Tuning the reactivities of metal−oxygen intermediates by redox-inactive metal ions has attracted interest in the bioinorganic chemistry for decades.[66−72] Based on the previous work for the Co^{III}−peroxo species with a tetradentate macrocyclic ligand, $[Co^{III}(TBDAP)(O_2)]^+$ (**1**^{TBDAP}), it is known that weak Lewis acids play an important role in nitrile activation.[44] To expand our understanding of the nitrile activation reaction, the addition of a weaker Lewis acid such as $Y(OTf)_3$ to a solution of **1** in CH_3CN/CH_3OH (v/v = 1:1) at 30 °C was examined, which resulted in the decay of **1** with the simultaneous production of corresponding **3** (70% yield) with an isosbestic point at 565 nm (Supporting Information, Figure S15a,b). The color changed from purple to cyan. The resulting solution was analyzed with ESI−MS, which exhibited an appreciable ion peak at m/z 190.6, corresponding to **3**, $[Co^{III}(Me_3\text{-TPADP})(CH_3C(=NH)O_2)]^{2+}$ (calcd. m/z 190.6) (Supporting Information, Figure S15c). These results suggested that weak Lewis acids also promoted nitrile activation to form **3** without the observation of **2**.

The transformation of **1** to **3** followed first-order kinetics with the k_{obs} values increasing proportionally with the concentration of CH_3CN to give a second-order rate constant (k_2) of 3.0(1) × 10^{-4} M^{-1} s^{-1} at 30 °C (Figures 4a, S15 and S16). The temperature-dependent k_2 values in the range of 298−323 K yielded a linear Eyring plot, which determined the activation parameters of $\Delta H^{\ddagger}$ = 7.5(1) kcal mol^{-1} and $\Delta S^{\ddagger}$ = −50(3) cal mol^{-1} K^{-1} (Figure 4b). Notably, the observed entropy value was much more negative than that of **2**. The second-order kinetics and the large negative entropy value suggested a bimolecular mechanism.

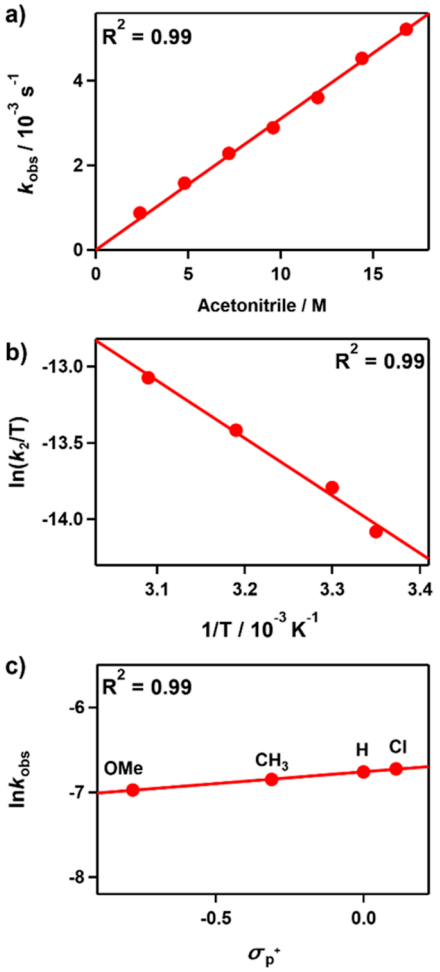

Figure 4. Reactivity studies of **1** (0.25 mM) with nitrile derivatives in the presence of $Y(OTf)_3$ (0.25 mM). (a) Plot of k_{obs} against the CH_3CN concentration to determine a second-order rate constant (k_2) at 30 °C. (b) Plot of second-order rate constants against $1/T$ to determine activation parameters. (c) Hammett plot of ln k_{obs} against σ_p^+ of benzonitrile derivatives, *para*-X−Ph−CN (X = OMe, CH_3, H, Cl) at 30 °C.

Addition of $Y(OTf)_3$ to a solution of **1** in the presence of 0.3 M PhCN in $CH_3OH/CHCl_3$ (v/v = 19:1) at 30 °C afforded **3**^{Ph} in 94% yield, which exhibited an isosbestic point at 592 nm (Figure S17 for UV−vis and ESI−MS spectra). Reactions of **1** with *para*-X−Ph−CN (X = MeO, CH_3, H, Cl) were performed, and the resulting Hammett plot of the pseudo-first-order rate constants versus σ_p^+ gave a ρ value of 0.25(3) (Figure 4c). The very small ρ value demonstrated that the electron-donating ability of the nitrile derivatives rarely affected the activation.[44]

The effect of M^{n+} ions was confirmed using relatively weaker Lewis acidic metal ions such as Lu^{3+} and Eu^{3+} instead of Y^{3+} (Figure S18). The logarithms of the pseudo-first-order rate constants (log k_{obs}) were correlated with the Lewis acidities of the metal ions, which revealed that the more Lewis acidic

https://doi.org/10.1021/jacsau.3c00532
JACS Au 2023, 3, 3204−3212

metals lead to faster rates (Figure S19). However, when the reaction was studied with more Lewis acid metals, Sc^{3+} and Al^{3+}, to further confirm the influence of the M^{n+} ions, a different outcome was observed; **1** was immediately converted to **2**. These results were nearly paralleled with the previously reported nitrile activation of $\mathbf{1}^{TBDAP}$ by weak Lewis acids.[44]

Mechanistic Studies

On the basis of the kinetic studies, the plausible mechanisms for the nitrile activation by **1** with weak and strong Lewis acids are illustrated in Scheme 3. Addition of weak Lewis acids such

Scheme 3. Proposed Mechanism of the Nitrile Activation Depending on the Lewis Acidity of M^{n+}

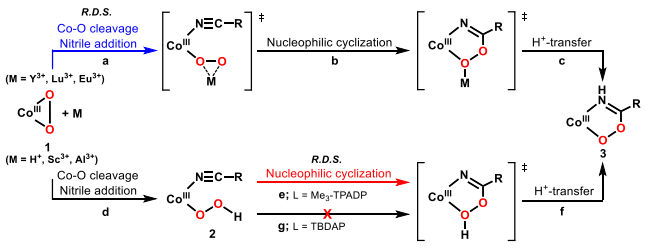

as Eu^{3+}, Lu^{3+}, and Y^{3+} to **1** resulted in the gradual conversion of **1** to **3**. It was proposed that the interaction of the peroxo moiety of **1** with weak Lewis acids promoted the Co−O bond cleavage with nitrile addition (step a). Subsequently, the nucleophilic attack of the peroxo ligand of **1** and the following H^+ transfer gave **3** (steps b and c) (Figure S20). The second-order kinetics and the low ρ value of 0.25(3) in Hammett analysis indicated that the Co−O bond cleavage process was a rate-determining step to form the end-on cobalt(III)−peroxo moiety, which was also supported by the trend of enhanced reaction rates with an increase of the Lewis acidity of M^{n+}. A similar mechanism has been proposed for the previously reported nitrile activation by the reaction of $\mathbf{1}^{TBDAP}$ and nitrile under the weak Lewis acids.[44]

In contrast, the treatment of the strong Lewis acid, HOTf, with **1** gave prompt formation of **2** (step d), which readily reacted with nitriles to form **3** (steps e and f). The observed first-order kinetics and the positive ρ value of 3.2(2) of **2** strongly supported that nitrile activation proceeded via a rate-determining intramolecular cyclization by the nucleophilic attack of distal oxygen on the hydroperoxo ligand to nitrile carbon (step e). The subsequent H^+ transfer reaction generated **3** (step f) (Figure S21).

The nitrile activation by **2** presented a marked difference with the previously reported cobalt(III)−hydroperoxo complex, $[Co^{III}(TBDAP)(O_2H)(CH_3CN)]^{2+}$ ($\mathbf{2}^{TBDAP}$), which showed a lack of reactivity with nitrile (step g).[44] To comprehend the distinct reactivity of nitrile activation, scrutinies of the crystal structures from the different ligand frameworks were employed. In the X-ray crystal structures of the cobalt(III)−peroxo complexes, **1** adopted a similar distorted octahedral geometry of $\mathbf{1}^{TBDAP}$, which arose from the substitutions of the two axial *tert*-butyl groups of $\mathbf{1}^{TBDAP}$ with methyl groups and one of the two equatorial pyridines with a tertiary amine.[44,57] However, the Co−N bond lengths of the two complexes displayed distinguished discrepancies. For instance, the average $Co-N_{ax}$ distance of 1.996 Å in **1** was significantly shorter than that of $\mathbf{1}^{TBDAP}$ (2.100 Å). The average $Co-N_{eq}$ of 1.951 Å in **1** was longer than the average $Co-N_{eq}$ of 1.879 Å in $\mathbf{1}^{TBDAP}$. The trends were very likely due to the presence of the steric bulkiness of the axial *tert*-butyl amine groups in $\mathbf{1}^{TBDAP}$, preventing the approach of axial ligands to the metal center. On the other hand, the less bulky methyl groups in **1** led to relatively contracted $Co-N_{ax}$ bonds, which probably pushed the equatorial ligands away. Similar effects of steric bulky substituents inducing longer M−N bond lengths have also been reported.[50−53]

Based on a comparison of the observed bond lengths of **1** and $\mathbf{1}^{TBDAP}$, thermodynamic parameters such as pK_a and redox potential of **2** were compared to those of $\mathbf{2}^{TBDAP}$. The pK_a value of **2** was estimated as 7.7, which was higher than that of $\mathbf{2}^{TBDAP}$ (pK_a = 2.1) (Figures S22 and S23). The significantly different pK_a values could be mainly rationalized by the compression of $Co-N_{ax}$ distances in Me_3-TPADP for the peroxo case, which could explain its higher basicity due to a strong ligand field.[44,57] Furthermore, the decreased redox potential of **2** (0.12 V vs $Fc^{+/0}$) compared to that of $\mathbf{2}^{TBDAP}$ (0.24 V vs $Fc^{+/0}$) indicated that **2** was a more electron-rich complex (Figure S24),[73] which was consistent with the previous studies that reported the decreases in redox potential values by the introduction of less bulky ligands.[50−53] These results were further supported by DFT calculations (vide infra). Thus, the substantially different pK_a values and redox potentials of **2** and $\mathbf{2}^{TBDAP}$ clearly illustrated that the control of basicity by ligand substitution greatly affected the nucleophilicity of the corresponding cobalt(III)−hydroperoxo complexes and regulated the reactivity of nitrile activation.

DFT Calculations

Previously, we reported the DFT calculations for **2** to obtain chemical insights into the geometry and O−O bond cleavage behavior.[56] In this work, to understand the difference in ligand field, we further studied the molecular orbitals (MOs) for the two cobalt(III)−hydroperoxo complexes **2** and $\mathbf{2}^{TBDAP}$ (Figure 5). The ground states of both **2** and $\mathbf{2}^{TBDAP}$ were determined to be $S = 0$, consistent with the experimental observation.[57,73] In the MO diagram, **2** shows a larger energy gap between the highest occupied molecular orbital (HOMO) and lowest unoccupied molecular orbital (LUMO) than that of $\mathbf{2}^{TBDAP}$.

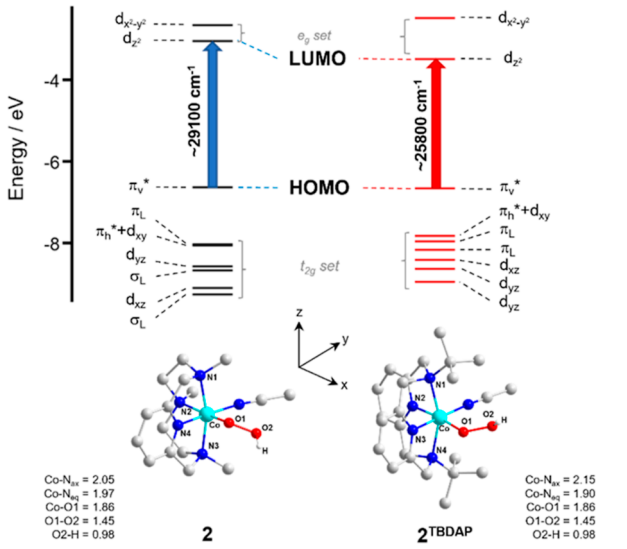

Figure 5. Molecular orbital diagrams for **2** and $\mathbf{2}^{TBDAP}$ (top) and optimized geometry (bottom).

https://doi.org/10.1021/jacsau.3c00532
JACS Au 2023, 3, 3204−3212

Both HOMOs dominantly originated from the π_v* orbital of peroxide (~85%) lying in similar energy so that the O−O bonds are less affected from the ligand field as shown in the O−O bond frequencies. In contrast, the LUMO of **2** is more destabilized compared to that of $\mathbf{2}^{TBDAP}$ with a large t_{2g}−e_g energy gap due to the majority of Co-d_{z^2} orbital being the constituent, which is reflected in the one-electron reduction potential. Moreover, a more stabilized $d_{x^2-y^2}$ orbital in **2** is consistent with the elongation of the equatorial donors (i.e., N2 and N4) by shortening of the axial donors of **2** (i.e., N1 and N3), inducing less splitting between the d_{z^2} and $d_{x^2-y^2}$ orbitals.[52,74,75] The contraction of the axial ligands in **2** is attributed to the less hindered methyl group rather than the bulkier *tert*-butyl substituent to the equatorial plan, by which the axial donors of **2** bind strongly to cobalt center. Therefore, the stronger ligand field of the Me_3-TPADP ligand of **2** than that of the TBDAP ligand of $\mathbf{2}^{TBADP}$ is ascribed not only to the substitution of the pyridine donor with an amine donor but also to the less bulky methyl group compared to the *tert*-butyl group.

Reaction of $[Co^{III}(Me_3\text{-TPADP})(CH_3C(=NH)O_2)]^{2+}$ (3) with Base

Upon adding 20 equiv of triethylamine (TEA) to the solution of **3** in CH_3CN at 60 °C, the decay of **3** was observed with the growth of an absorption band at 312 nm (ε = 4700 M^{-1} cm^{-1}) (Scheme 4 and Figure S25a). The ESI−MS spectrum of the

Scheme 4. Transformation Pathways for Cobalt(III)−Peroxyimidato Complex (3) with Triethylamine (TEA)

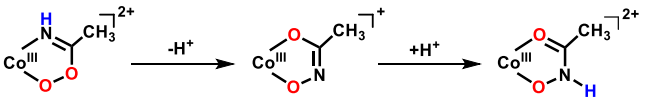

solution showed prominent peaks at m/z of 380.3 and 190.6. The main peak at m/z 380.3 corresponds to $[Co(Me_3\text{-TPADP})(CH_3(=NO)O)]^+$ (calcd. m/z 380.2), which indicated the formation of a cobalt(III)−hydroximato complex by the deprotonation of **3** (Figure S25b). The other peak at m/z 190.6 was consistent with the cobalt(III)−hydroxamato species, $[Co(Me_3\text{-TPADP})(CH_3C(-NHO)O)]^{2+}$ (calcd. m/z 190.6). The protonated form was favored in Me_3-TPADP, while the deprotonated form was preferred in TBDAP. The result agreed with the difference in the basicity of the cobalt(III)−hydroperoxo complexes.

CONCLUSIONS

In this study, we have shown that the addition of HOTf to the solution of a cobalt(III)−peroxo complex, $[Co^{III}(Me_3\text{-TPADP})(O_2)]^+$ (**1**), resulted in the formation of cobalt(III)−hydroperoxo complexes, $[Co^{III}(Me_3\text{-TPADP})(O_2H)(RCN)]^{2+}$ [R = Me (**2**) and Ph ($\mathbf{2}^{Ph}$)], conducting nitrile activation to yield cobalt(III)−peroxyimidato complexes, $[Co^{III}(Me_3\text{-TPADP})(R-C(=NH)O_2)]^{2+}$ [R = Me (**3**) and Ph ($\mathbf{3}^{Ph}$)]. **3** was characterized with various physicochemical methods such as UV−vis, ESI−MS, IR, NMR, EPR, and XRD analysis. The first-order kinetics and the positive ρ value of 3.2(2) in Hammett analysis demonstrated that the formation of **3** occurred via the intramolecular nucleophilic attack of the hydroperoxide ligand to the carbon atom of nitrile in **2**. In the reaction of **1** with nitrile in the presence of weak Lewis acids such as $Y(OTf)_3$, $Lu(OTf)_3$, and $La(OTf)_3$ instead of HOTf, the formation of **3** was observed with second-order kinetics, suggesting a bimolecular mechanism. The very low Hammett ρ value of 0.25(3) and the slower reaction rate with the weaker Lewis acids indicated that the Co−O bond cleavage was the rate-determining step. However, the previously reported cobalt(III)−hydroperoxo complex, $[Co^{III}(TBDAP)(O_2H)(CH_3CN)]^{2+}$ ($\mathbf{2}^{TBDAP}$), was unreactive with nitrile, showing a contrasting result to **2**. The analysis of the properties of **2** and $\mathbf{2}^{TBDAP}$ revealed that **2** had a higher pK_a value of 7.7 compared to that of $\mathbf{2}^{TBDAP}$ (pK_a = 2.1). The lower redox potential value of **2** (0.12 V vs $Fc^{+/0}$) in comparison to $\mathbf{2}^{TBDAP}$ (0.24 V vs $Fc^{+/0}$) agreed with the higher electron-donating ability of **2**. The DFT studies of **2** and $\mathbf{2}^{TBDAP}$ suggested that the stronger ligand field in **2** was primarily related to the shorter Co−N_{ax} bond distances by the introduction of a less bulky methyl group, in line with the results from the crystal structures of the cobalt(III)−peroxo complexes of Me_3-TPADP and TBDAP. This study provided the first mechanistic elucidations into nitrile activation by the cobalt(III)−hydroperoxo complex and shed light on the crucial role of basicity in nitrile activation.

METHODS

The following analytical instruments and software were used in this study: UV−vis: Hewlett-Packard 8454 diode array, ESI−MS: Waters Acquity SQD Quadrupole, FT-IR: Thermo Scientific Nicolet iS10, EPR: JEOL JES-FA200, NMR: Varian VNMRS 600, CV: CH Instruments, CHI 600E, XRD: Bruker SMART APEX II CCD, and DFT calculations: Gaussian 09 computational package.

ASSOCIATED CONTENT

Supporting Information

The Supporting Information is available free of charge at https://pubs.acs.org/doi/10.1021/jacsau.3c00532.

Experimental details on the generation and characterization and DFT calculations; UV−vis, ESI−MS, IR, EPR, NMR data (^{1}H, ^{13}C, ^{1}H−^{1}H COSY, ^{1}H−^{13}C HSQC), and X-ray diffraction analysis of **3**; kinetic procedures and data; UV−vis titration for pK_a values of **2** and $\mathbf{2}^{TBDAP}$; and cyclic voltammogram for **2** (PDF)

Crystallographic data of $[Co^{III}(Me_3\text{-TPADP})(CH_3C(=NH)O_2)](ClO_4)_2(CH_3CN)_2$ (CIF)

AUTHOR INFORMATION

Corresponding Author

Jaeheung Cho − *Department of Chemistry, Ulsan National Institute of Science and Technology (UNIST), Ulsan 44919, Republic of Korea; Graduate School of Carbon Neutrality, Ulsan National Institute of Science and Technology (UNIST), Ulsan 44919, Republic of Korea;* orcid.org/0000-0002-2712-4295; Email: jaeheung@unist.ac.kr

Authors

Yeongjin Son − *Department of Chemistry, Ulsan National Institute of Science and Technology (UNIST), Ulsan 44919, Republic of Korea; Department of Emerging Materials Science, Daegu Gyeongbuk Institute of Science and Technology (DGIST), Daegu 42988, Republic of Korea*

Donghyun Jeong − *Department of Chemistry, Ulsan National Institute of Science and Technology (UNIST), Ulsan 44919, Republic of Korea*

Kyungmin Kim − *Department of Chemistry, Ulsan National Institute of Science and Technology (UNIST), Ulsan 44919,*

https://doi.org/10.1021/jacsau.3c00532
JACS Au 2023, 3, 3204−3212

Republic of Korea; Department of Emerging Materials Science, Daegu Gyeongbuk Institute of Science and Technology (DGIST), Daegu 42988, Republic of Korea; orcid.org/0000-0002-3362-128X

Complete contact information is available at: https://pubs.acs.org/10.1021/jacsau.3c00532

Notes

The authors declare no competing financial interest.

■ ACKNOWLEDGMENTS

This research was supported by the Korea Drug Development Fund funded by the Ministry of Science and ICT (MSIT), Ministry of Trade, Industry, and Energy, and Ministry of Health and Welfare (RS-2023-00217242). This work was supported by the National Research Foundation of Korea funded by the MSIT (RS-2023-00259920).

■ REFERENCES

(1) Kobayashi, M.; Shimizu, S. Nitrile Hydrolases. *Curr. Opin. Chem. Biol.* **2000**, *4*, 95−102.
(2) Varela, J. A.; Saá, C. Construction of Pyridine Rings by Metal-Mediated [2 + 2 + 2] Cycloaddition. *Chem. Rev.* **2003**, *103*, 3787−3802.
(3) Chin, J. Developing Artificial Hydrolytic Metalloenzymes by a Unified Mechanistic Approach. *Acc. Chem. Res.* **1991**, *24*, 145−152.
(4) Eglin, J. L. Nitrile Hydrolysis Promoted by Rhenium(III) Metal-Metal Bonded Systems. *Comments Inorg. Chem.* **2002**, *23*, 23−43.
(5) Kukushkin, V. Y.; Pombeiro, A. J. L. Additions to Metal-Activated Organonitriles. *Chem. Rev.* **2002**, *102*, 1771−1802.
(6) Kukushkin, V. Y.; Pombeiro, A. J. L. Metal-Mediated and Metal-Catalyzed Hydrolysis of Nitriles. *Inorg. Chim. Acta* **2005**, *358*, 1−21.
(7) Murakami, T.; Nojiri, M.; Nakayama, H.; Dohmae, N.; Takio, K.; Odaka, M.; Endo, I.; Nagamune, T.; Yohda, M. Post-Translational Modification is Essential for Catalytic Activity of Nitrile Hydratase. *Protein Sci.* **2000**, *9*, 1024−1030.
(8) Kovacs, J. A. Synthetic Analogues of Cysteinate-Ligated Non-Heme Iron and Non-Corrinoid Cobalt Enzymes. *Chem. Rev.* **2004**, *104*, 825−848.
(9) Bork, P.; Koonin, E. V. A New Family of Carbon-Nitrogen Hydrolases. *Protein Sci.* **1994**, *3*, 1344−1346.
(10) Brennan, B. A.; Alms, G.; Nelson, M. J.; Durney, L. T.; Scarrow, R. C. Nitrile Hydratase from *Rhodococcus rhodochrous* J1 Contains a Non-Corrin Cobalt Ion with Two Sulfur Ligands. *J. Am. Chem. Soc.* **1996**, *118*, 9194−9195.
(11) Payne, M. S.; Wu, S.; Fallon, R. D.; Tudor, G.; Stieglitz, B.; Turner, I. M. J. R.; Nelson, M. J. A Stereoselective Cobalt-Containing Nitrile Hydratase. *Biochemistry* **1997**, *36*, 5447−5454.
(12) Brenner, C. Catalysis in the Nitrilase Superfamily. *Curr. Opin. Struct. Biol.* **2002**, *12*, 775−782.
(13) Hopmann, K. H. Full Reaction Mechanism of Nitrile Hydratase: A Cyclic Intermediate and an Unexpected Disulfide Switch. *Inorg. Chem.* **2014**, *53*, 2760−2762.
(14) Zinn, P. J.; Sorrell, T. N.; Powell, D. R.; Day, V. W.; Borovik, A. S. Acetonitrile Hydration and Ethyl Acetate Hydrolysis by Pyrazolate-Bridged Cobalt(II) Dimers Containing Hydrogen-Bond Donors. *Inorg. Chem.* **2007**, *46*, 10120−10132.
(15) Ahmed, T. J.; Knapp, S. M. M.; Tyler, D. R. Frontiers in Catalytic Nitrile Hydration: Nitrile and Cyanohydrin Hydration Catalyzed by Homogeneous Organometallic Complexes. *Coord. Chem. Rev.* **2011**, *255*, 949−974.
(16) Swartz, R. D.; Coggins, M. K.; Kaminsky, W.; Kovacs, J. A. Nitrile Hydration by Thiolate- and Alkoxide-Ligated Co-NHase Analogues. Isolation of Co(III)-Amidate and Co(III)-Iminol Intermediates. *J. Am. Chem. Soc.* **2011**, *133*, 3954−3963.
(17) Vogt, M.; Nerush, A.; Iron, M. A.; Leitus, G.; Diskin-Posner, Y.; Shimon, L. J. W.; Ben-David, Y.; Milstein, D. Activation of Nitriles by Metal Ligand Cooperation. Reversible Formation of Ketimido- and Enamido-Rhenium PNP Pincer Complexes and Relevance to Catalytic Design. *J. Am. Chem. Soc.* **2013**, *135*, 17004−17018.
(18) Mukherjee, A.; Srimani, D.; Chakraborty, S.; Ben-David, Y.; Milstein, D. Selective Hydrogenation of Nitriles to Primary Amines Catalyzed by a Cobalt Pincer Complex. *J. Am. Chem. Soc.* **2015**, *137*, 8888−8891.
(19) Stevenson, D. E.; Wright, J. N.; Akhtar, M. Mechanistic Consideration of P-450 Dependent Enzymic Reactions: Studies on Oestriol Biosynthesis. *J. Chem. Soc., Perkin Trans. 1* **1988**, *7*, 2043−2052.
(20) Watanabe, Y.; Ishimura, Y. A Model Study on Aromatase Cytochrome P-450 Reaction: Transformation of Androstene-3,17,19-trione to 10.Beta.-hydroxyester-4-ene-3,17-dione. *J. Am. Chem. Soc.* **1989**, *111*, 8047−8049.
(21) Watanabe, Y.; Ishimura, Y. Aromatization of tetralone derivatives by 5,10,15,20-tetrakis(pentafluorophenyl)-porphyrinatoiron(III) chloride/iodosobenzene and cytochrome P-450cam: a model study on aromatase cytochrome P-450 reaction. *J. Am. Chem. Soc.* **1989**, *111*, 410−411.
(22) Cole, P. A.; Bean, J. M.; Robinson, C. H. Conversion of a 3-Desoxysteroid to 3-Desoxyestrogen by Human Placental Aromatase. *Proc. Natl. Acad. Sci. U.S.A.* **1990**, *87*, 2999−3003.
(23) Karlsson, A.; Parales, J. V.; Parales, R. E.; Gibson, D. T.; Eklund, H.; Ramaswamy, S. Crystal Structure of Naphthalene Dioxygenase: Side-on Binding of Dioxygen to Iron. *Science* **2003**, *299*, 1039−1042.
(24) Gibson, D. T.; Parales, R. E. Aromatic Hydrocarbon Dioxygenases in Environmental Biotechnology. *Curr. Opin. Biotechnol.* **2000**, *11*, 236−243.
(25) Wertz, D. L.; Sisemore, M. F.; Selke, M.; Driscoll, J.; Valentine, J. S. Mimicking Cytochrome P-450 2B4 and Aromatase: Aromatization of a Substrate Analogue by a Peroxo Fe(III) Porphyrin Complex. *J. Am. Chem. Soc.* **1998**, *120*, 5331−5332.
(26) Goto, Y.; Wada, S.; Morishima, I.; Watanabe, Y. Reactivity of Peroxoiron(III) Porphyrin Complexes: Models for Deformylation Reactions Catalyzed by Cytochrome P-450. *J. Inorg. Biochem.* **1998**, *69*, 241−247.
(27) Seo, M. S.; Kim, J. Y.; Annaraj, J.; Kim, Y.; Lee, Y.-M.; Kim, S.-J.; Kim, J.; Nam, W. $[Mn(tmc)(O_2)]^+$: A Side-on Peroxido Manganese(III) Complex Bearing a Non-Heme Ligand. *Angew. Chem., Int. Ed.* **2007**, *46*, 377−380.
(28) Annaraj, J.; Cho, J.; Lee, Y.-M.; Kim, S. Y.; Latifi, R.; de Visser, S. P.; Nam, W. Structural Characterization and Remarkable Axial Ligand Effect on the Nucleophilic Reactivity of a Nonheme Manganese(III)-Peroxo Complex. *Angew. Chem., Int. Ed.* **2009**, *48*, 4150−4153.
(29) Cho, J.; Sarangi, R.; Kang, H. Y.; Lee, J. Y.; Kubo, M.; Ogura, T.; Solomon, E. I.; Nam, W. Synthesis, Structural, and Spectroscopic Characterization and Reactivities of Mononuclear Cobalt(III)-Peroxo Complexes. *J. Am. Chem. Soc.* **2010**, *132*, 16977−16986.
(30) Cho, J.; Sarangi, R.; Nam, W. Mononuclear Metal-O_2 Complexes Bearing Macrocyclic N-Tetramethylated Cyclam Ligands. *Acc. Chem. Res.* **2012**, *45*, 1321−1330.
(31) Cho, J.; Jeon, S.; Wilson, S. A.; Liu, L. V.; Kang, E. A.; Braymer, J. J.; Lim, M. H.; Hedman, B.; Hodgson, K. O.; Valentine, J. S.; Solomon, E. I.; Nam, W. Structure and Reactivity of a Mononuclear Non-Haem Iron(III)-Peroxo Complex. *Nature* **2011**, *478*, 502−505.
(32) Kim, J.; Shin, B.; Kim, H.; Lee, J.; Kang, J.; Yanagisawa, S.; Ogura, T.; Masuda, H.; Ozawa, T.; Cho, J. Steric Effect on the Nucleophilic Reactivity of Nickel(III) Peroxo Complexes. *Inorg. Chem.* **2015**, *54*, 6176−6183.
(33) Jeong, D.; Selverstone Valentine, J.; Cho, J. Bio-inspired mononuclear nonheme metal peroxo complexes: Synthesis, structures and mechanistic studies toward understanding enzymatic reactions. *Coord. Chem. Rev.* **2023**, *480*, 215021−215060.

(34) Bayston, J. H.; Winfield, M. E. A Mononuclear Hydroperoxo Complex and its Significance in Catalytic Oxidation Mechanisms. *J. Catal.* **1964**, *3*, 123−128.
(35) Guzei, I. A.; Bakac, A. Macrocyclic Hydroperoxocobalt(III) Complex: Photochemistry, Spectroscopy, and Crystal Structure. *Inorg. Chem.* **2001**, *40*, 2390−2393.
(36) Kim, D.; Cho, J.; Lee, Y.-M.; Sarangi, R.; Nam, W. Synthesis, Characterization, and Reactivity of Cobalt(III)-Oxygen Complexes Bearing a Macrocyclic N-Tetramethylated Cyclam Ligand. *Chem.—Eur. J.* **2013**, *19*, 14112−14118.
(37) Sankaralingam, M.; Lee, Y.-M.; Jeon, S. H.; Seo, M. S.; Cho, K.-B.; Nam, W. A Mononuclear Manganese(III)-Hydroperoxo Complex: Synthesis by Activating Dioxygen and Reactivity in Electrophilic and Nucleophilic Reactions. *Chem. Commun.* **2018**, *54*, 1209−1212.
(38) Bae, S. H.; Li, X.-X.; Seo, M. S.; Lee, Y.-M.; Fukuzumi, S.; Nam, W. Tunneling Controls the Reaction Pathway in the Deformylation of Aldehydes by a Nonheme Iron(III)-Hydroperoxo Complex: Hydrogen Atom Abstraction versus Nucleophilic Addition. *J. Am. Chem. Soc.* **2019**, *141*, 7675−7679.
(39) Kim, B.; Jeong, D.; Ohta, T.; Cho, J. Nucleophilic Reactivity of a Copper(II)-Hydroperoxo Complex. *Commun. Chem.* **2019**, *2*, 81−86.
(40) Zhao, R.; Zhang, B.-B.; Liu, Z.; Cheng, G.-J.; Wang, Z.-X. DFT Mechanistic Insights into Aldehyde Deformylations with Biomimetic Metal-Dioxygen Complexes: Distinct Mechanisms and Reaction Rules. *JACS Au* **2022**, *2*, 745−761.
(41) Noh, H.; Jeong, D.; Ohta, T.; Ogura, T.; Valentine, J. S.; Cho, J. Distinct Reactivity of a Mononuclear Peroxocobalt(III) Species toward Activation of Nitriles. *J. Am. Chem. Soc.* **2017**, *139*, 10960−10963.
(42) Cho, D.; Choi, S.; Cho, J.; Baik, M.-H. Peroxocobalt(III) Species Activates Nitriles via a Superoxocobalt(II) Diradical State. *Dalton Trans.* **2020**, *49*, 2819−2826.
(43) Zhao, R.; Guo, J.; Zhang, C.; Lu, Y.; Dagnaw, W. M.; Wang, Z.-X. DFT Mechanistic Insight into the Dioxygenase-Like Reactivity of a Co^{III}-Peroxo Complex: O-O Bond Cleavage via a [1,3]-Sigmatropic Rearrangement-Like Mechanism. *Inorg. Chem.* **2020**, *59*, 2051−2061.
(44) Kim, K.; Cho, D.; Noh, H.; Ohta, T.; Baik, M.-H.; Cho, J. Controlled Regulation of the Nitrile Activation of a Peroxocobalt(III) Complex with Redox-Inactive Lewis Acidic Metals. *J. Am. Chem. Soc.* **2021**, *143*, 11382−11392.
(45) Miyaji, T.; Kujime, M.; Hikichi, S.; Moro-oka, Y.; Akita, M. Synthesis and Characterization of a Series of (Hydroperoxo)-(Alkylperoxo)-and (μ-Peroxo)palladium Complexes Containing the Hydrotris(3,5-diisopropylpyrazolyl)borato Ligand (Tp^{iPr2}): (Tp^{iPr2})-(py)Pd-OO-X [X = H, *t*-Bu, Pd(Tp^{iPr2})(py)] and (Tp^{iPr2})(py)Pd-(μ-κ^1:κ^2-OO)-PdTp^{iPr2}. *Inorg. Chem.* **2002**, *41*, 5286−5295.
(46) Li, L.; Narducci Sarjeant, A. A.; Vance, M. A.; Zakharov, L. N.; Rheingold, A. L.; Solomon, E. I.; Karlin, K. D. Exogenous Nitrile Substrate Hydroxylation by a New Dicopper-Hydroperoxide Complex. *J. Am. Chem. Soc.* **2005**, *127*, 15360−15361.
(47) Müller, J.; Würtele, C.; Walter, O.; Schindler, S. Transformation of Nitrile to Cyanide and Aldehyde Using a Cobalt(II) Complex and Dioxygen. *Angew. Chem., Int. Ed.* **2007**, *46*, 7775−7777.
(48) Bittner, A.; Braun, T.; Herrmann, R.; Mebs, S. Rhodium-Mediated Oxygenation of Nitriles with Dioxygen: Isolation of Rhodium Derivatives of Peroxyimidic Acids. *Chem.—Eur. J.* **2015**, *21*, 12299−12302.
(49) Caneschi, A.; Dei, A. Promoted Hydrolysis of Nitriles using Hydrogen Peroxide: the Isolation and the Characterization of a Paramagnetic Nickel(II)-Peroxoacetimido Derivative. *Inorg. Chim. Acta* **1988**, *141*, 3−4.
(50) Zang, Y.; Kim, J.; Dong, Y.; Wilkinson, E. C.; Appelman, E. H.; Que, L. Models for Nonheme Iron Intermediates: Structural Basis for Tuning the Spin States of Fe(TPA) Complexes. *J. Am. Chem. Soc.* **1997**, *119*, 4197−4205.
(51) Saravanan, N.; Sankaralingam, M.; Palaniandavar, M. Manganese(II) complexes of tetradentate 4N ligands with diazepane backbones for catalytic olefin epoxidation: effect of nucleophilicity of peroxo complexes on reactivity. *RCS Adv.* **2014**, *4*, 12000−12011.
(52) Massie, A. A.; Denler, M. C.; Cardoso, L. T.; Walker, A. N.; Hossain, M. K.; Day, V. W.; Nordlander, E.; Jackson, T. A. Equatorial Ligand Perturbations Influence the Reactivity of Manganese(IV)−Oxo Complexes. *Angew. Chem., Int. Ed.* **2017**, *56*, 4178−4182.
(53) Tang, F.; Qu, F.; Khusnutdinova, J. R.; Rath, N. P.; Mirica, L. M. Structural and Reactivity Comparison of Analogous Organometallic Pd(III) and Pd(IV) complexes. *Dalton Trans.* **2012**, *41*, 14046−14050.
(54) Selke, M.; Sisemore, M. F.; Valentine, J. S. The Diverse Reactivity of Peroxy Ferric Porphyrin Complexes of Electron-Rich and Electron-Poor Porphyrins. *J. Am. Chem. Soc.* **1996**, *118*, 2008−2012.
(55) Selke, M.; Valentine, J. S. Switching on the Nucleophilic Reactivity of a Ferric Porphyrin Peroxo Complex. *J. Am. Chem. Soc.* **1998**, *120*, 2652−2653.
(56) Shin, B.; Sutherlin, K. D.; Ohta, T.; Ogura, T.; Solomon, E. I.; Cho, J. Reactivity of a Cobalt(III)-Hydroperoxo Complex in Electrophilic Reactions. *Inorg. Chem.* **2016**, *55*, 12391−12399.
(57) Son, Y.; Kim, K.; Kim, S.; Tripodi, G. L.; Pereverzev, A.; Roithová, J.; Cho, J. Spectroscopic Evidence for a Cobalt-Bound Peroxyhemiacetal Intermediate. *JACS Au* **2021**, *1*, 1594−1600.
(58) Sakharov, S. G.; Zarelua, S. A.; Kokunov, Y. V.; Buslaev, Y. A. Tungsten(VI) Fluoride Dimethylhydrazide Complexes: η^2 and η^1 Isomerism. *Inorg. Chem.* **1992**, *31*, 3302−3305.
(59) McEwen, I.; Ahlberg, P. Direct Observation of Intramolecular Hydrogen Bonding of a Hydroxy Proton to an Indenide Carbanion in Apolar and Polar Non-Hydrogen Bond Donor Solvents by NMR and IR Spectroscopy. *J. Am. Chem. Soc.* **1992**, *114*, 10869−10873.
(60) Meschede, L.; Gerritzen, D.; Limbach, H.-H. Dynamic NMR Study of the Interference between Cyclic Proton Exchange, Selfassociation and Hindered Rotation of Diphenylformamidine in Tetrahydrofuran. *Ber Bunsenges Phys Chem.* **1988**, *92*, 469−485.
(61) Bertini, I.; Lanini, G.; Luchinat, C.; Messori, L.; Monnanni, R.; Scozzafava, A. Investigation of Cu_2Co_2SOD and its Anion Derivatives. Proton NMR and Electronic Spectra. *J. Am. Chem. Soc.* **1985**, *107*, 4391−4396.
(62) Li, Y.; Marks, T. J. Organolanthanide-Catalyzed Intramolecular Hydroamination/Cyclization of Aminoalkynes. *J. Am. Chem. Soc.* **1996**, *118*, 9295−9306.
(63) Leitch, D. C.; Platel, R. H.; Schafer, L. L. Mechanistic Elucidation of Intramolecular Aminoalkene Hydroamination Catalyzed by a Tethered Bis(ureate) Complex: Evidence for Proton-Assisted C-N Bond Formation at Zirconium. *J. Am. Chem. Soc.* **2011**, *133*, 15453−15463.
(64) Pouy, M. J.; Delp, S. A.; Uddin, J.; Ramdeen, V. M.; Cochrane, N. A.; Fortman, G. C.; Gunnoe, T. B.; Cundari, T. R.; Sabat, M.; Myers, W. H. Intramolecular Hydroalkoxylation and Hydroamination of Alkynes Catalyzed by Cu(I) Complexes Supported by *N*-Heterocyclic Carbene Ligands. *ACS Catal.* **2012**, *2*, 2182−2193.
(65) Lepori, C.; Gómez-Orellana, P.; Ouharzoune, A.; Guillot, R.; Lledós, A.; Ujaque, G.; Hannedouche, J. Well-Defined β-Diketiminatocobalt(II) Complexes for Alkene Cyclohydroamination of Primary Amines. *ACS Catal.* **2018**, *8*, 4446−4451.
(66) Rohde, J.-U.; In, J.-H.; Lim, M. H.; Brennessel, W. W.; Bukowski, M. R.; Stubna, A.; Münck, E.; Nam, W.; Que, L. Crystallographic and Spectroscopic Characterization of a Nonheme Fe(IV)=O Complex. *Science* **2003**, *299*, 1037−1039.
(67) Lee, Y.-M.; Bang, S.; Kim, Y. M.; Cho, J.; Hong, S.; Nomura, T.; Ogura, T.; Troeppner, O.; Ivanović-Burmazović, I.; Sarangi, R.; Fukuzumi, S.; Nam, W. A Mononuclear Nonheme Iron(III)-Peroxo Complex Binding Redox-Inactive Metal Ions. *Chem. Sci.* **2013**, *4*, 3917−3923.
(68) Li, F.; Van Heuvelen, K. M.; Meier, K. K.; Münck, E.; Que, L. Sc^{3+}-Triggered Oxoiron(IV) Formation from O_2 and its Non-Heme Iron(II) Precursor via a Sc^{3+}-Peroxo-Fe^{3+} Intermediate. *J. Am. Chem. Soc.* **2013**, *135*, 10198−10201.

https://doi.org/10.1021/jacsau.3c00532
JACS Au 2023, 3, 3204−3212

(69) Bang, S.; Lee, Y.-M.; Hong, S.; Cho, K.-B.; Nishida, Y.; Seo, M. S.; Sarangi, R.; Fukuzumi, S.; Nam, W. Redox-Inactive Metal Ions Modulate the Reactivity and Oxygen Release of Mononuclear Non-Haem Iron(III)-Peroxo Complexes. *Nat. Chem.* **2014**, *6*, 934−940.
(70) Nam, W. Synthetic Mononuclear Nonheme Iron-Oxygen Intermediates. *Acc. Chem. Res.* **2015**, *48*, 2415−2423.
(71) Bae, S. H.; Lee, Y. M.; Fukuzumi, S.; Nam, W. Fine Control of the Redox Reactivity of a Nonheme Iron(III)-Peroxo Complex by Binding Redox-Inactive Metal Ions. *Angew. Chem., Int. Ed.* **2017**, *56*, 801−805.
(72) Kim, B.; Kim, S.; Ohta, T.; Cho, J. Redox-Inactive Metal Ions That Enhance the Nucleophilic Reactivity of an Alkylperoxocopper-(II) Complex. *Inorg. Chem.* **2020**, *59*, 9938−9943.
(73) Kim, K.; Oh, S.; Jeong, D.; Lee, Y.; Moon, D.; Lee, S.; Cho, J. Systematic Electronic Tuning on the Property and Reactivity of Cobalt-(Hydro)peroxo Intermediates. *Inorg. Chem.* **2023**, *62*, 7141−7149.
(74) Geiger, R. A.; Chattopadhyay, S.; Day, V. W.; Jackson, T. A. A Series of Peroxomanganese(III) Complexes Supported by Tetradentate Aminopyridyl Ligands: Detailed Spectroscopic and Computational Studies. *J. Am. Chem. Soc.* **2010**, *132*, 2821−2831.
(75) Geiger, R. A.; Wijeratne, G.; Day, V. W.; Jackson, T. A. Steric and Electronic Influences on the Structures of Peroxomanganese(III) Complexes Supported by Tetradentate Ligands. *Eur. J. Inorg. Chem.* **2012**, *2012*, 1598−1608.

https://doi.org/10.1021/jacsau.3c00532
JACS Au 2023, 3, 3204−3212